Vol 15 No 12, December 2006
1009-1963/2006/15(12)/2989-11

Chinese Physics

© 2006 Chin. Phys. Soc.
and IOP Publishing Ltd

Experimental characteristics of a lower hybrid wave multi-junction coupler in the HT-7 tokamak *

Ding Bo-Jiang(丁伯江)†, Shan Jia-Fang(单家方), Liu Fu-Kun(刘甫坤), Fang Yu-De(方瑜德), Wei Wei(韦 维), Wu Zhen-Wei(吴振伟), Chen Zhong-Yong(陈忠勇), Xu Han-Dong(徐汉东), Wang Mao(王 茂), Jiang Min(蒋 敏), Zhang Gong-Rang(张公让), Huang Feng(黄 峰), Zhao Yan-Ping(赵燕平), Kuang Guang-Li(匡光力), and HT-7 team

Institute of Plasma Physics, Chinese Academy of Sciences, Hefei 230031, *China*

(Received 17 March 2006; revised manuscript received 7 August 2006)

A phase-controlled lower hybrid wave (LHW) multi-junction (MJ) coupler (3(rows)×4(columns)×4 (subwaveguides)) has been developed in the HT-7 tokamak. Simulations show that it is more effective for driving plasma current than an ordinary phase-controlled LHW antenna (3(rows)× 12(columns)) (traditional coupler). The plasma–wave coupling experiments show that the reflection coefficient (RC) is below 10%, implying that the MJ grill can launch the wave into the plasma effectively. The effect of power spectrum launched by the MJ coupler on RC indicates that an optimal condition is requisite for a better coupling in the lower hybrid current drive (LHCD) experiments. Studies indicate that the drive efficiency of the MJ antenna is higher than that of the traditional one, which is mainly ascribed to the discrepancy in impurity concentration, plasma temperature, and spectrum directivity. An improved confinement with an electron internal transport barrier is obtained by LHCD. The analysis shows that the modified negative (low) magnetic shear and the change of radial electric field profile due to LHCD are possible factors responsible for the eITB formation.

Keywords: antenna, plasma heating, plasma confinement
PACC: 5240F, 5250G, 5255

1. Introduction

Lower hybrid current drive (LHCD) is an effective way to drive plasma current and modify plasma current profile, and thereby improve plasma confinement in a tokamak. The relevant results have been reported in many tokamak devices, such as JT-60U, JET, Tore-supra, FTU,[1−4] and the HT-7 superconducting tokamak.[5−11] A 1.2 MW (12 × 100 kW) LHCD system[12] with 12 klystron amplifiers operating at a frequency $f = 2.45$ GHz has been installed in the HT-7 tokamak to drive plasma current. The wave generated by the system is fed into the tokamak by an antenna, which is one of the key factors determining launched spectrum, hence it can affect wave propagation, power deposition, and current drive efficiency, consequently, the plasma confinement is affected. So it is essential to study the antenna's property.

The MJ coupler is being considered to drive the plasma current in the international tokamak experiment reactor (ITER) device. Relevant pre-experiments for ITER with this kind of antenna have been reported in JT-60U,[13] Tore-supra[14] and JET,[15,16] and further work is underway in FTU with a passive-active multijunction (PAM).[17] To achieve a high-performance plasma, a phase-controlled LHW MJ coupler (3(rows) ×4 (columns)×4(subwaveguides)) has been developed[18] in the HT-7 tokamak since 2001. By means of the newly developed MJ coupler, an improved confinement[9] with an internal transport barrier (ITB) formation characterized by an ion temperature profile has been reported, and its capability to modify plasma current has been demonstrated. Also, the edge plasma fluctuation suppression by LHCD with the MJ coupler has been analysed.[10,11] Here, we intend to investigate the characteristics of the MJ grill, the wave–plasma coupling characteristics, and the current drive efficiency for two types of antennae (MJ and traditional grills[19] (3(rows)× 12(columns), where each module is not divided into subwaveguide with a fixed

*Project supported by the National Natural Science Foundation of China (Grant Nos 10205015 and 10575104).
†E-mail: bjding@ipp.ac.cn

phase difference, see Section 2)), and analyse the improved confinement with electron ITB formation. In the experiments, deuterium serves as the working gas.

2. Characteristics of the multi-junction grill

The HT-7 superconducting tokamak[20] is a middle-sized (major radius: 1.22 m, minor radius: 0.28 m) limiter configuration device with a circular cross-section. The launcher mouth structure is designed to match the plasma shape so that the effect of this mismatch on the wave–plasma coupling should be reduced as much as possible. As shown in Fig.1, the traditional coupler with an L_G of 18.32 cm (L_G is the width of the grill) consists of 12 waveguides per row in two rows, which had been utilized in experiments before 2001, while the MJ grill (L_G= 19.3 cm) consists of 12 modules arranged in an array of 3 rows and 4 columns, and each module is divided into 4 waveguides with a fixed phase difference ($\sim 90°$) resulting from a built-in phase shifter in between and is supplied by a single power source. Therefore, in each row there would be 16 waveguides. The power spectra (see Ref.[21]) launched by the MJ and the traditional coupler are shown in Fig.2, in which magnifications of the main lobes for the two couplers are superimposed and $N_{//}^{\rm peak}$ denotes the peak value of the parallel refractive index of the main lobe.

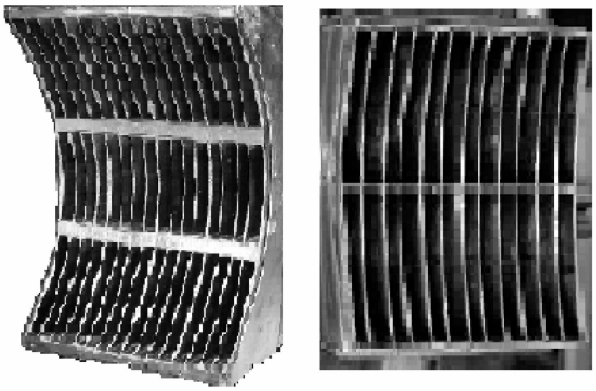


Fig.1. Structure of grill mouth (left: MJ, right: traditional).

It is seen that the traditional coupler has an asymmetric spectrum with a half-width at half maximum $\Delta_{\rm HFWD} \sim 0.62$, while the MJ grill has a more asymmetric one with a narrower half-width ($\Delta_{\rm HFWD} \sim 0.59$), which is beneficial to the current drive and controlling current profile, partly at the expense of its heating electron capacity. With the reflection coefficient assumed to be 0.1, the $N_{//}$-weighted ($N_{//}$ denotes the parallel refractive index) directivity[22] based on the theoretical current drive efficiency of the waves is 0.714 for the MJ grill and 0.567 for the traditional one, indicating that the MJ grill can offer more efficient current drive power. In order to compare the drive capabilities of the two couplers, a ray tracing code[23] is utilized to calculate the wave power deposition, from which a non-inductive current can further be estimated by using a two-dimensional Fokker–Planck equation.[23] In the code, the positive and the negative components of the spectrum are both considered, for the driven current by LHCD is determined by the waves propagating in both co- and counter-direction. For simplicity, it is assumed that the mechanism of interaction between plasma and waves with positive and negative parallel refractive indices is the same (i.e. the quasilinear Landau damping is used in both cases, whereas the electron interacting with the waves propagating in the co- and counter-direction moves along the opposite direction), but the driven currents are in opposite directions.

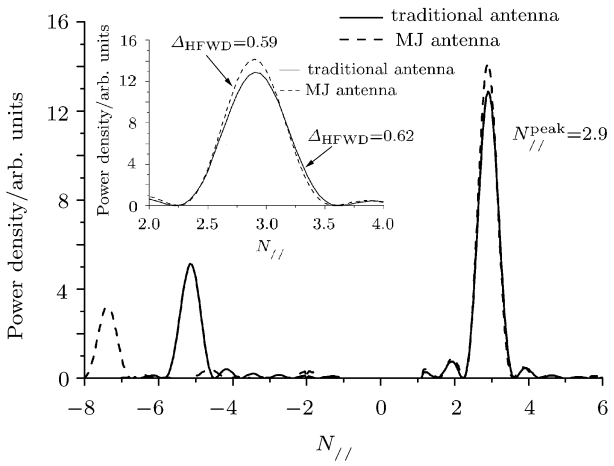


Fig.2. Spectra launched by MJ and traditional antennae.

Using the ray-tracing code, with plasma parameters assumed to be in the same form (density and temperature profiles are both assumed to be parabolic) and the spectra shown in Fig.2, the simulated power deposition profiles in Fig.3(a) show that there exists little difference in the deposition contributed by the positive spectrum component between the MJ coupler and the traditional one, whereas for the contributions from the negative spectrum component there

is a prominent difference between the two antennae. The different peak positions in the two negative cases mainly result from the different power spectra in the side lobe. The further calculated driven current profiles shown in Fig.3(b) indicate that the driven current is larger in the MJ case, meaning the higher drive efficiency of the MJ grill due to its better directivity.

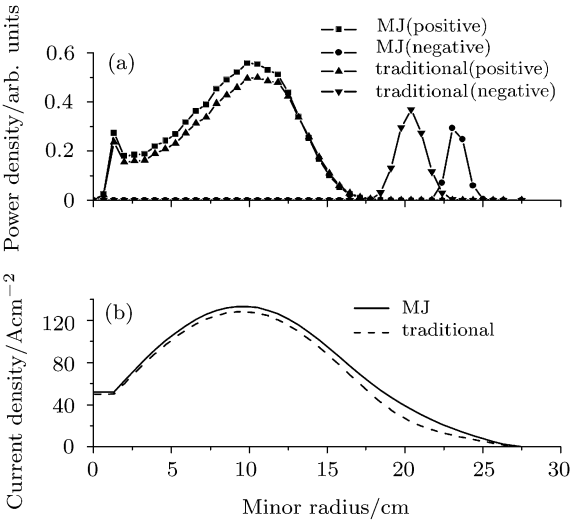


Fig.3. Simulated results for the spectra (shown in Fig.2) launched by MJ and traditional antennas, (a) power deposition for the positive/negative spectra, (b) driven current.

With the developed MJ grill, the launched spectra in the main lobe with different phase differences ($\Delta\Phi$) between the modules are shown in Fig.4, in which with the increasing phase difference, the peaks of parallel refractive index of the power maximum shift towards large values. The asymmetric spectra offer a necessity to effectively drive non-inductive plasma current. The variation of $N_{//}^{\rm peak}$ enables the wave to control plasma current profile by adjusting its spectrum purposely. The relationship between $N_{//}^{\rm peak}$ and $\Delta\Phi$ is illustrated in Table 1, from which we can see that the relation between $N_{//}^{\rm peak}$ and $\Delta\Phi$ is nearly in accord with the analytic equation ($N_{//}^{\rm peak} = n_{//0}[1 + \Delta\Phi/360°]$, $n_{//0}$ is the $N_{//}^{\rm peak}$ value when $\Delta\Phi = 0$) given by Litaudon and Moreau.[24]

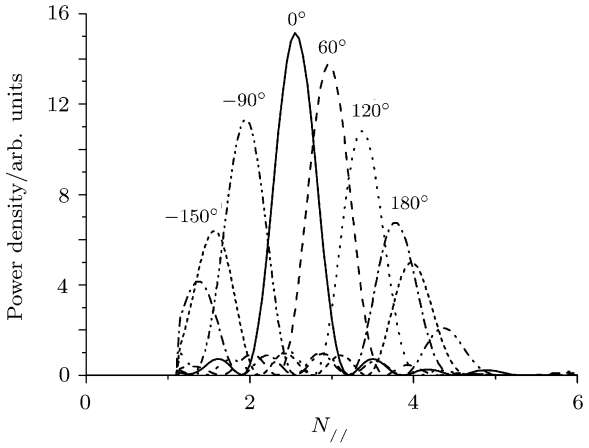


Fig.4. Main lobe spectra launched by the MJ antenna with different phase differences ($\Delta\Phi$) between adjacent modules.

Table 1. Relationship between $N_{//}^{\rm peak}$ and $\Delta\Phi$ for the spectrum launched by the MJ antenna.

$\Delta\Phi/(°)$	−150	−120	−90	−60	−30	0	30	60	90	120	150	180
$N_{//}^{\rm peak}$	1.55	1.75	1.95	2.15	2.35	2.55	2.75	2.95	3.15	3.35	3.55	3.8

3. Wave–plasma coupling experiments

Using the MJ coupler, plasma–wave coupling experiments with a plasma current $I_{\rm p}$ ∼120 kA are performed by both scanning plasma density with $N_{//}^{\rm peak} \sim 2.55$ and scanning $\Delta\Phi$ from −150 to 180^0 (correspondingly, $N_{//}^{\rm peak}$ varies from 1.55 to 3.8), with a central line averaged density ($n_{\rm e}$) being $1.0\times10^{19}{\rm m}^{-3}$. The reflection coefficient, which is a main indicator of wave–plasma coupling and determined by a bi-directional coupler, can be roughly estimated by the ratio between the reflected power and the incident power ($P_{\rm re}/P_{\rm in}$). The results displayed in Fig.5 show that the reflection coefficient (RC) is below 10% so good coupling efficiencies are obtained for both scanning cases, indicating that the MJ grill can effectively couple the wave into the plasma for the present HT-7 experiments. In particular, within the measurement error-bar, low reflections are observed in the range of $1.75 \le N_{//}^{\rm peak} \le 3.35$, beyond which the reflection increases, suggesting that an optimal spectrum is requisite for a better coupling.

The grill-mouth density,

$$n_{\rm e,grill} = n_{\rm e,LCFS} \cdot \exp\Big(-\frac{d}{\lambda_{\rm SOL}}\Big),$$

determined by the distance d between the last closed flux surface (LCFS) and the grill mouth, plays a dom-

inant role in determining the wave–plasma coupling. Here, $n_{\mathrm{e,LCFS}}$ and λ_{SOL} are the density at the LCFS and the decay length in the scrape-off layer, respectively, measured by Langmuir probes. Wave–plasma coupling requires the plasma density at the grill mouth to be above a cut-off density determined by $n_{\mathrm{e,co}} = (\omega^2 m_{\mathrm{e}})/(4\pi e^2)$, where ω is the wave frequency, m_{e} the electron mass and e the electron charge. Otherwise, the coupling will deteriorate and the reflection will increase, hence giving rise to an arc in a waveguide. More specifically, for a good coupling an optimal density required at the antenna aperture is given by $n_{\mathrm{e,grill}}^{\mathrm{opt}} \geq N_{//}^2 n_{\mathrm{e,co}}$.[25] For the HT-7 tokamak, the cut-off density at a frequency of 2.45 GHz is about 7.4 $\times 10^{16}$ m^{-3}, and the plasma density at the grill mouth is about $1.5 \times 10^{18} \times \exp(-1.5/1.0) \sim 3.23 \times 10^{17}$ m^{-3}. The low reflections for the density and the spectrum scan experiments suggest that the plasma density in front of the grill mouth satisfies the coupling condition, which is demonstrated by the above estimation. This is mainly because the grill is very close ($d \sim 1.5$ cm) to the LCFS plasma and the decay length ($\lambda_{\mathrm{SOL}} \sim 1.0$ cm) is not too small, the ratio d/λ_{SOL} is not large enough to reduce the mouth density to the cut-off value. With the density varying, the change of reflection is not so obvious as in the case of the spectrum. This indicates that once the coupling condition is satisfied, the dependence of coupling on density is weak, which has also been reported in Tore-supra.[14] It is still not understood why a small increase in reflection at the density of 1.9×10^{19} m^{-3} is observed. According to the Brambilla theory,[21] on condition that the edge density is not so large that the high heat flux occurs, the increasing density will be beneficial to the wave–plasma coupling. Whether this is caused by the measurement error or due to the change of density gradient in front of the antenna is not yet known.

The effect of power spectrum launched by MJ coupler on reflection, which has been reported experimentally and theoretically in Tore-Supra,[22] is possibly due to the high harmonic $N_{//}$ components of LHW spectrum.[26,27] The interaction between these components and the electrons in the edge region gives rise to high heat loads, leading to the formation of hot spots on the plasma facing components as reported in some devices[16,28,29] and large impurity influxes, which deteriorate the coupling and the plasma quality. In addition, with the increase of $N_{//}$, the optimal coupling condition is satisfied not very well. This is another reason for the deterioration of the coupling when $N_{//}^{\mathrm{peak}} > 3.35$.

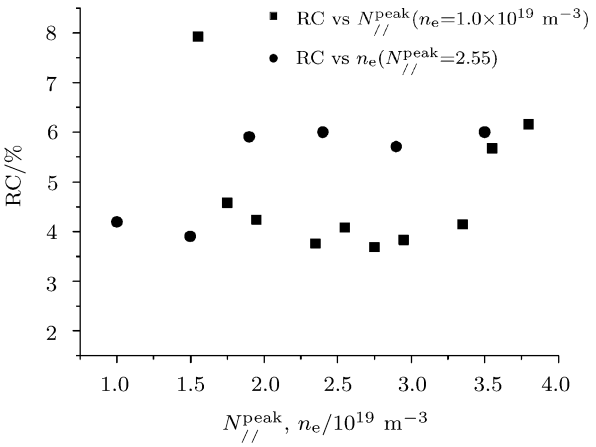


Fig.5. Dependence of reflection coefficient on spectrum and density.

4. Current drive efficiency

The current drive efficiency of the MJ antenna is also investigated by scanning plasma density ($n_{\mathrm{e}} \sim$ 1.0, 1.5, 2.0 ($\times 10^{19}$ m^{-3}) with a phase difference of $\Delta\Phi = 60$ between adjacent modules ($N_{//}^{\mathrm{peak}} = 2.95$). The experiments are performed with the parameters $I_{\mathrm{p}} \sim 150$ kA, $B_{\mathrm{t}} \sim 1.9$ T, and $P_{\mathrm{LHW}} \sim 350$ kW. As done in the study of the traditional antenna, the experiments are performed with a feedback control system that adjusts the input power from the ohmic (OH) transformer so as to keep plasmas current I_{p} constant. The current drive efficiency is evaluated by the formula [30]

$$\eta_{\mathrm{cd}}^{\mathrm{exper}} = \frac{n_{\mathrm{e}} I_{\mathrm{rf}} R_{\mathrm{p}}}{P_{\mathrm{rf}}}, \tag{1}$$

where R_{p} is the major radius of tokamak and P_{rf} is the LH wave power absorbed by plasma through Landau damping. The driven current I_{rf} is approximated by $I_{\mathrm{rf}} = (\Delta V/V_{\mathrm{OH}}) \cdot I_{\mathrm{p}}$, with the effects of the Spitzer resistivity and the hot conductivity neglected, where $\Delta V = V_{\mathrm{OH}} - V_{\mathrm{LH}}$, V_{OH} is the loop voltage in the OH heating phase just before applying the LH power, and V_{LH} is the loop voltage during the LHCD phase. Figure 6(a) shows the effects of the power spectrum and the plasma density on the current drive efficiency for the present MJ grill. In order to compare the experimental current drive capabilities of the two couplers, the dependence of current drive efficiency on plasma density with $N_{//}^{\mathrm{peak}} = 2.9$ for the traditional antenna, which was studied in [7] is also presented in the figure.

It is seen that the best drive efficiency is obtained at a density of 1.5×10^{19} m^{-3} in the MJ case. Though the experimental data are very limited, a comparison between the results from the traditional and MJ antennae shows that both the antennae have an optimal density region where good drive efficiency can be obtained. Analysis[7] indicates that this is partly determined by the competition between the wave accessibility condition and impurity concentration ($Z_{\rm eff}$). High electron density means that more wave beams cannot enter the core plasma due to the accessibility condition and the impurity concentration increases in the case of low electron density. As a result, according to the theoretical formula derived from Fisch's theory,[30,31] we have

$$\eta_{\rm cd}^{\rm theor} = 1240/[\ln \Lambda (5 + Z_{\rm eff}) < N_{//}^2 >], \qquad (2)$$

with

$$\frac{1}{\langle N_{//}^2 \rangle} = \frac{\int_{N_{//\rm acc}}^{+\infty} P(N_{//})/N_{//}^2 \mathrm{d}N_{//} - \int_{-\infty}^{-N_{//\rm acc}} P(N_{//})/N_{//}^2 \mathrm{d}N_{//}}{\int_{-\infty}^{+\infty} P(N_{//}) \mathrm{d}N_{//}}. \qquad (3)$$

Naturally, the good drive efficiency is available in an optimal density range. Here, $P(N_{//})$ is the power spectrum of the launched LHW, $N_{//\rm acc}$[32] the critical value of the parallel refractive index, and Λ the Coulomb logarithm.

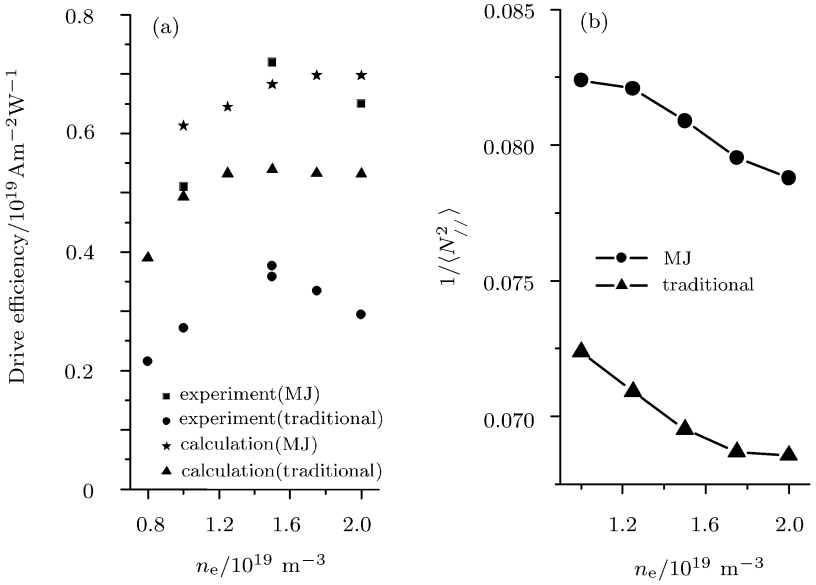


Fig.6. Dependence of (a) drive efficiency and (b) calculated $1/\langle N_{//}^2 \rangle$ on density for the two launchers.

Further comparison shows that in the whole density range, the drive efficiency of the MJ antenna is higher than that of the traditional one, indicating that the MJ grill is more effective to drive current than the traditional coupler. Simulations in Section 2 show that one possible reason for the difference in drive efficiency between the two antennae is that the MJ coupler drives a larger fraction of non-inductive current because of its more asymmetric spectrum, i.e. better directivity. Of course, this may not completely account for the experimental discrepancy in drive efficiency between the two couplers, for, as shown in Fig.6(a), the efficiency of the MJ coupler is almost twice that of the traditional one and the simulation shows that the discrepancy in spectrum directivity cannot lead to so great a difference. Other physical behaviour in the discharge, such as impurity radiation, or electron temperature $T_{\rm e}$, could be also responsible for the large discrepancy in the drive efficiency. The experimentally obtained drive efficiency in JT-60 and

JET devices[33] is given as

$$\eta_{\rm CD} = \frac{\langle T_{\rm e}\rangle}{5 + Z_{\rm eff}} C(N_{//}), \qquad (4)$$

which indicates that the drive efficiency strongly depends on impurity concentration and temperature. Here, $C(N_{//})$ $(= 1240/[\ln \Lambda < N_{//}^2 >])$ is correlated with the LHCD power spectrum, $\langle T_{\rm e}\rangle$ is the volume averaged electron temperature. For the MJ antenna, the estimated values of $Z_{\rm eff}$ from the impurity radiation before the LHCD application are shown in Fig.7, in which also shown are the values[7] in the case of the traditional antenna. It is seen that in the low electron density region, the $Z_{\rm eff}$ values are in line with part of the curve in the case of the traditional antenna, while with the electron density increasing, they deviate from the results in the case of the traditional antenna gradually and become smaller and smaller. This brings on a higher drive efficiency in the high electron density region, but it does not do so in the low electron density plasma. This means that, though $Z_{\rm eff}$ in the case of the MJ grill is smaller than that in the case of the traditional one in the high density plasma, it also only partly explains the difference in drive efficiency. Since antenna-launched power spectrum and impurity concentration cannot explain the experimental results completely, according to Eqs.(2) and (3), it is inferred that $T_{\rm e}$ may be used to explain the higher drive efficiency. Unfortunately, not enough measurements of $T_{\rm e}$ are available to analyse the above result further.

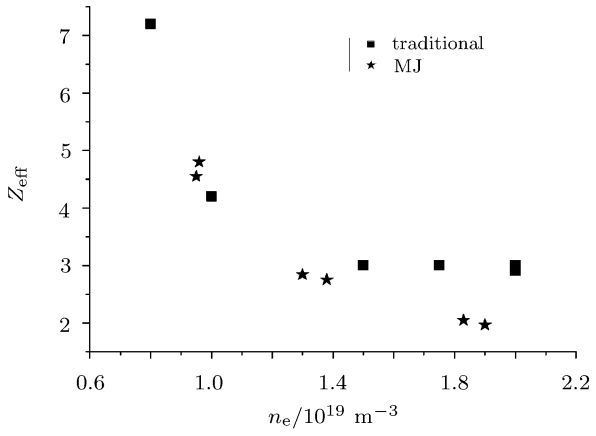


Fig.7. Dependence of $Z_{\rm eff}$ on $n_{\rm e}$.

The higher efficiencies of the MJ grill are quantitatively in agreement with those obtained in the JT-60U tokamak[13] with the same LHW frequency as that in HT-7. It is reported[13] that the efficiency of the MJ launcher is 40% higher than that of the previous traditional launcher. However, a maximum value of 2.8×10^{19} A·W^{-1}·m^{-2} is obtained in JT-60U for the MJ grill, much larger than 0.72×10^{19} A·W^{-1}·m^{-2} for our case. This is mainly due to the difference in plasma temperature, routinely, which is much higher in JT-60U than in HT-7.

With the two power spectra used in our experiment, the calculated values of $1/\langle N_{//}^2\rangle$ through Eq.(3) are also shown in Fig.6(b), suggesting that the better drive efficiency of the MJ grill is ascribed to its better directivity. It is seen that the value of $1/\langle N_{//}^2\rangle$ decreases with the increasing density, meaning that the wave accessibility becomes poorer and the drive efficiency affected by the accessibility condition decreases at high electron densities. With the measured $Z_{\rm eff}$ as shown in Fig.7, the calculated current drive efficiencies for the cases of the two antennae through Eq.(2) are shown in Fig.6(a), indicating that the drive efficiency in the MJ case is larger than that in the traditional antenna case. The calculations for the two cases do not decrease as the experimental data do in the high electron density region. This discrepancy may be ascribed to the limitation of Fisch's theory, in which electron temperature is not taken into account. The temperature in the high electron density case is lower than that in the low electron density case because the slowing-down time becomes shorter at higher electron densities. Therefore, the temperature is another factor responsible for decreasing the experimental drive efficiency at high electron densities.

5. Electron ITB formation by LHCD

LHCD is an effective tool for improving confinement by means of internal transport barrier (ITB) formation. Figure 8 shows a typical waveforms of LHCD experiment (#60452) performed with the MJ coupler with the following parameters $I_{\rm p} \sim 150$ kA, $B_{\rm T} \sim 1.9$ T, $n_{\rm e} \sim 1.0 \times 10^{19}$ m^{-3} $P_{\rm LHW} \sim 300$ kW, and $N_{//}^{\rm peak} = 2.55$. It is seen that after the onset of LHW (see Fig.8(a)), the loop voltage $V_{\rm p}$ decreases from 1.3 to 0.3 V (see Fig.8(b)), implying that about 115 kA current is maintained by LHCD. The central electron temperature $T_{\rm e}(0)$ (see Fig.8(c)), derived from a soft x-ray energy spectrum analyser,[34,35] increases from ~ 1.0 to $\sim$1.5 keV, implying that part of wave beams propagate into the core region plasma and transfer their energy to the core electrons through Landau

damping, which is partly supported by the central chord hard x-ray radiation (H-x-ray) intensity (see Fig.8(b)) due to bremsstrahlung emission. The increases in $T_e(0)$ and the central line averaged density n_e, measured by an HCN laser, together with no obvious change in impurity radiation (I. R.) (see Fig.8(d)), lead to an enhanced intensity of soft x-ray radiation (S-x-ray) as indicated in Fig.8(d). In addition, a drastic drop in the neutral deuterium emission (D_α) (see Fig.8(f)) when the LHW is input, and a slight increase in n_e at the time of D_α drop indicate an improvement on particle confinement because of LHCD, for no increase in the injected working gas (I.G.) (see Fig.8(e)) is observed after the LHCD application.

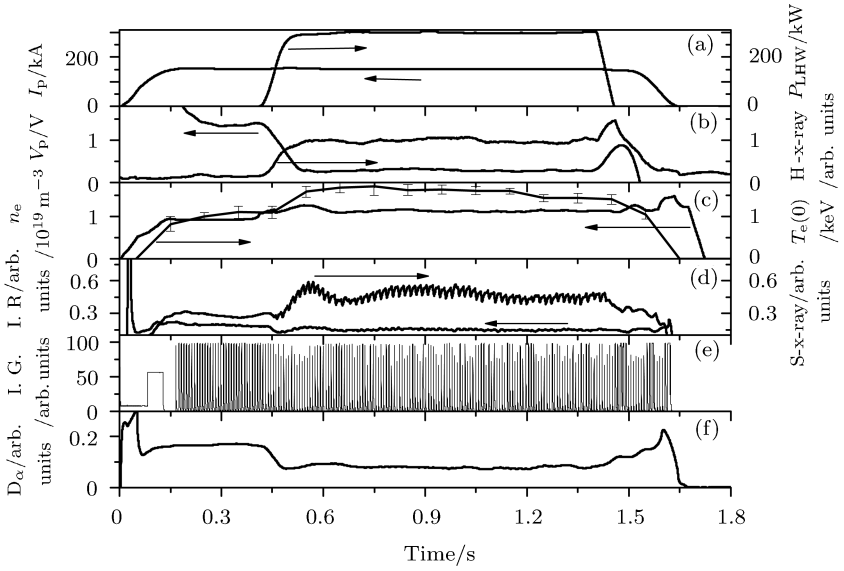


Fig.8. Typical waveforms of LHCD experiment (#60452). (a) I_p: plasma current, P_{LHW}: LHW power; (b) V_p: plasma loop voltage, H-x-ray: intensity of hard x-ray radiation; (c) $T_e(0)$: central electron temperature, n_e: central line averaged plasma density; (d) I.R.: intensity of impurity radiation, S-x-ray: intensity of soft x-ray radiation; (e) I.G.: injected working gas; (f) D_α: neutral deuterium emission.

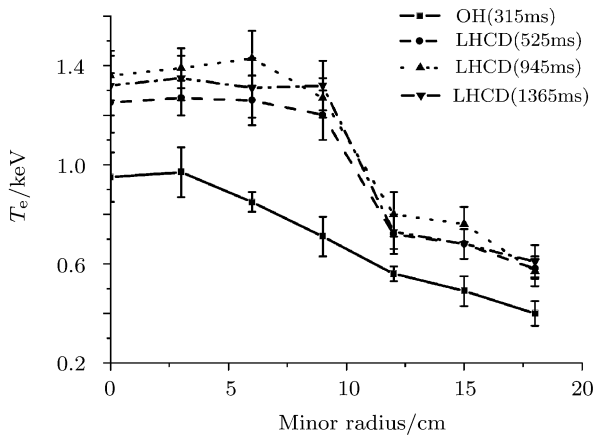


Fig.9. Electron temperature profiles in OH and LHCD phases.

The electron temperature profiles with a space resolution of 0.03 m in the OH and the LHCD phases are deduced (see Fig.9) from an analysis of bremsstrahlung radiation in the soft x-ray region.[34,35] It is seen that comparing with T_e in the OH phase, T_e in the LHCD phase increases in the whole radial region, and the increase in the inner region (< 10.0 cm) is much larger than that in the outer region. The universal increase implies that (1) the accessibility condition is satisfied and wave is able to reach the core region, and (2) the wave beams have enough energy to enter the core region after the absorption in the outer region, which is mainly because of a multi-pass absorption occurring during the ray propagation due to low $N_{//}$ and not too high T_e. The different increases in T_e at different radial positions may be ascribed to different power depositions at the different locations. The drastic increase in T_e in the inner region implies that most of the LHW power is absorbed by the core electrons, as identified by the simulated power deposition (Fig.10(a)) through the code simulation.[23] It is due to this different increases in T_e at different positions that an obvious increase of the T_e profile gradient in the range of $9.0 \sim 12.0$ cm is observed. According to the criterion[36] characterized by the T_e gradient, an electron ITB (eITB) is formed in this case. It is seen that within the measurement

error-bar a stationary eITB is achieved in the LHCD phase from the T_e profile at the different time-slices as shown in Fig.9, meaning that an improved confinement with eITB is obtained by LHCD.

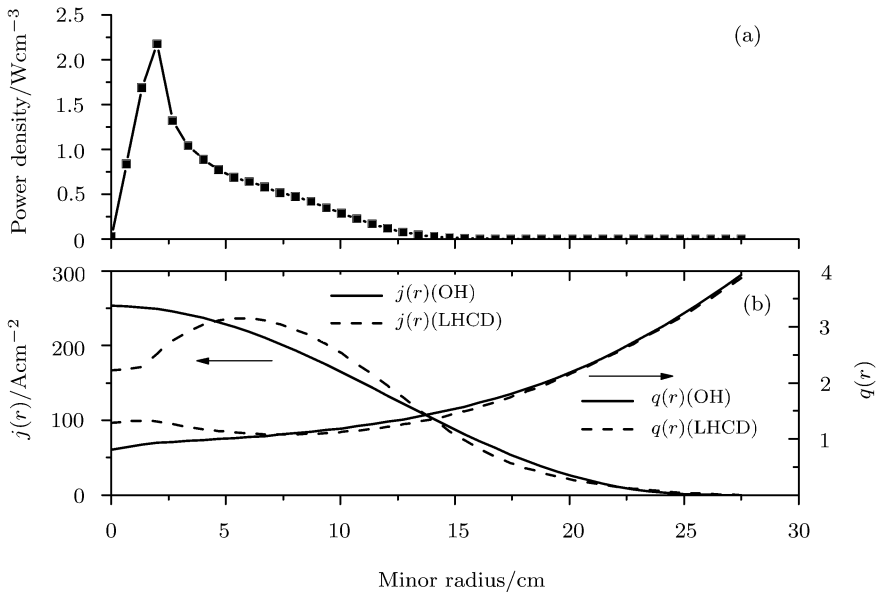


Fig.10. Simulation results with the experiment parameters (#60452) (a) power deposition profile (b) profiles of current density ($j(r)$) and $q(r)$ in OH and LHCD phases.

One of the possible factors responsible for the eITB formation is the changed magnetic shear. The magnetic shear is expressed as $s = r/q(\mathrm{d}q/\mathrm{d}r)$, where q is the safety factor and r the radius of the magnetic surface. Experiments on JET and modelling show that the q-profile plays an important role in eITB formation.[3,37−39] Code simulations indicate that an ITB could form in the presence of a strong negative magnetic shear[40−42] or in the vicinity of low-order rational q surfaces with a small magnetic shear ($s \sim 0$).[43] Using the experimental parameters and assuming a parabolic ohmic current profile, the calculated profiles of current density and q in the OH and LHCD phases are displayed in Fig.10(b), showing that a hollow current profile forms due to LHCD. As a result, as shown by the q profile in Fig.10(b), a reversed magnetic shear in the centre is obtained in the LHCD phase. The q minimum ($q_{\min}$) where $s \sim 0$ is around unit and located at the position of $r/a \sim 0.75$ that is near to the eITB. A similar result has been obtained in JT-60U.[44] Also, this is almost consistent with the result that an ITB forms in many cases in JET when $q_{\min}$ crosses a low-order rational number[3,37,38,45] in the vicinity of the $s = 0$ region. Experimental results in this paper show that an eITB is formed in HT-7. The simulations suggest that a central negative magnetic shear or a low magnetic shear in the low-order rational surface possibly forms because of the hollow current profile. Though there exists some uncertainty in our calculation, the experimental results can be interpreted by the calculations according to the code simulation.[40−43] From this point, the form of eITB could result from the negative (low) magnetic shear due to the modified current profile by LHCD.

Another possible mechanism for the formation of eITB is the shear of radial electric field. It is shown theoretically and experimentally[46] that the flow of $\boldsymbol{E}_r \times \boldsymbol{B}$($E_r$ is the radial electric field, and B is the magnetic field) drift is responsible for plasma transport and that it is a main factor responsible for an improvement in the plasma confinement. Evidence that a flow-shear-induced transport barrier can be produced in a core plasma using injected radio frequency waves has also been reported.[47] Since an enhanced shear flow is beneficial to improving confinement, the formation of eITB in our case could be correlated with the change in E_r because of LHCD. The reduction in electron transport coefficients (χ_e) is beneficial to the eITB formation. Study[48] has shown that χ_e reduces with enhancing E_r shear, suggesting that the E_r shear plays a role in forming the eITB. Since electrons are accelerated by LHW in the toroidal direction and LHCD

has little effect on the poloidal velocity of electrons, the radial electric field must be modified so as to keep the electrons' forces balanced. Based on the radial equilibrium of electrons that are considered as an object in discussion below, E_r can be simulated by the following expression:[49]

$$E_r = -\frac{1}{en_e}(\nabla P_e + JB_\theta), \tag{5}$$

where ∇P_e is the gradient of electron pressure, J the plasma current density, and B_θ the poloidal magnetic field. Note that in order to see the effect of LHCD on radial electric field, E_r here includes only a pressure term and toroidal rotation term, for LHW mainly accelerates the electrons in the toroidal direction and has little influence on the poloidal rotation. Figure 11(a) displays the calculated E_r profiles in the OH phase (E_r(OH)) and LHCD phase (E_r(LHCD)), and the change of radial electric field (ΔE_r) due to LHCD. This figure shows a notched structure in ΔE_r, which is created due to LHCD. The E_r drop deepens the ΔE_r notched structure and changes the E_r shear. The values of dE_r/dr are also calculated as shown in Fig.11(b). It is seen that $|(dE_r/dr)|$ dominating $\omega_{E_r\times B}$ increases gradually on the both sides of ∼10 cm. As the increased shear approaches the maximum of the turbulent linear growth rate, i.e. $\omega_{E_r\times B} \geq \gamma_{max}$,[50,51] or the nonlinear turbulent decorrelation rate, i.e. $\omega_{E_r\times B} \geq \Delta\omega_D$,[52,53] an improved confinement with an eITB formation can be obtained. Furthermore, it is seen that the maximum values of $|(dE_r/dr)|$ in LHCD are located at the positions of ∼ 5 cm and 12.5 cm, which span the interval covering the ITB region indicated by the T_e profile. Therefore, it is speculated that the change of radial electric field profile due to LHCD could be another factor responsible for the eITB formation.

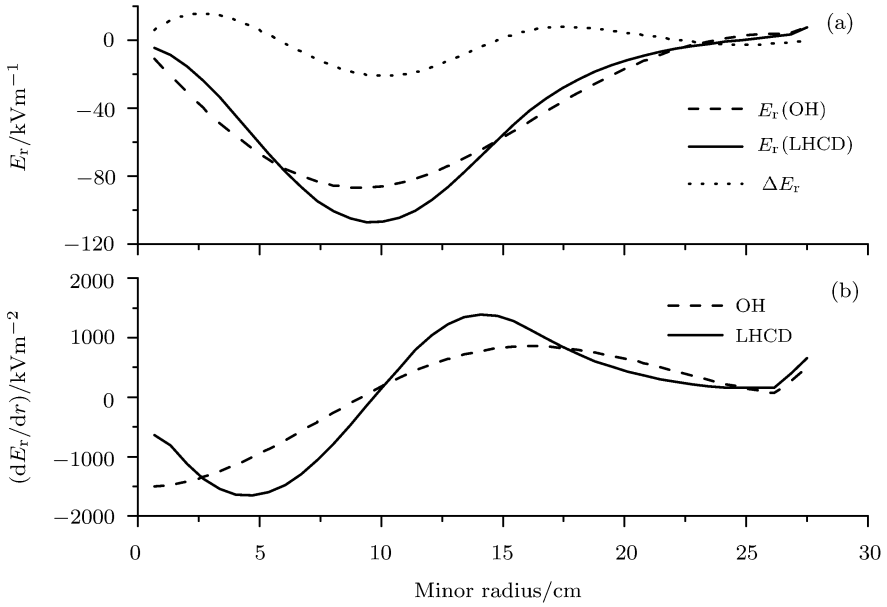


Fig.11. Simulated profiles of (a) radial electric field and (b) its shear in OH and LHCD phases.

Though the above two explanations are mainly based on the simulation due to a lack of measurements, according to the present theory the calculations may interpret our experimental results, i.e. the modified negative (low) magnetic shear and the changed E_r shear are two possible factors responsible for the eITB formation. Unfortunately, there are not enough documented data available to estimate the magnetic shear and E_r shear for the present.

It seems that, from the simulation, the magnetic shear and the E_r shear ($E_r \times B$ shear) are coincidental in determining the eITB formation. More work is needed to demonstrate it.

6. Conclusions

A phase-controlled LHW MJ coupler has been developed in the HT-7 tokamak. Simulations show that it is more effective to drive plasma current than a traditional coupler due to its better directivity. The plasma–wave coupling experiments show that good coupling efficiencies with a low reflection coefficient

below 10% are obtained, indicating that the wave can be effectively launched into the plasma by the MJ grill in our experiments. The spectrum scan experiment shows that an optimal spectrum is requisite for a better coupling.

The investigations of the capability of current drive of the MJ antenna show that there exists an optimal density region where a good drive efficiency is obtained, which is mainly determined by the wave accessibility condition, impurity concentration, and electron temperature. For a certain density, the drive efficiency of the MJ antenna is higher than that of the traditional one. Studies indicate that impurity concentration, plasma temperature, and spectrum directivity could be responsible for the higher drive efficiency of the MJ coupler.

An improved confinement with an eITB, indicated by T_e profile, is obtained by LHCD. It is inferred from the simulation that the modified negative (low) magnetic shear and the change of radial electric field profile due to LHCD could be the possible responsible for the eITB formation.

All of the studies suggest that the newly developed MJ coupler in the HT-7 tokamak is effective to couple the wave power into plasma, to drive current, and to modify current profile, and thereby to improve plasma confinement.

Acknowledgement

One of the authors, Ding B J, would like to thank the members of HT-7 Team for their cooperation and kindly help.

References

[1] Hoang G T, Gil C, Joffrin E *et al* 1994 *Nucl. Fusion* **34** 75

[2] Ide S, Fujita T, Naito O *et al* 1996 *Plasma Phys. Control. Fusion* **38** 1645

[3] Pamela J and JET EFDA Contributors 2003 *Nucl. Fusion* **43** 1540

[4] Romanelli F FTU Team and ECRH Team 2002 *Overview of the FTU Results Fusion Energy* 2002 (*Proc. 19th Int. Conf. Lyon, 2002)* (Vienna: IAEA) CD-ROM file OV/4-5 and http://www.iaea.org/programmes/ripc/physics/fec2002/html/fec2002.htm

[5] Kuang G L, Xu W H, Zhang X Q *et al* 1998 *Chin. Phys. Lett.* **15** 435

[6] Kuang G L, Liu Y X, Shan J F *et al* 1999 *Nucl. Fusion* **39** 1769

[7] Ding B J, Kuang G L, Liu Y X *et al* 2000 *Chin. Phys. Lett.* **17** 519

[8] Shen W C, Kuang G L, Liu Y X *et al* 2000 *Plasma Sci. Technol.* **2** 227

[9] Ding B J, Kuang G L, Shan J F *et al* 2003 *Nucl. Fusion* **43** 558

[10] Ding B J, Kuang G L, Liu Y X *et al* 2004 *Phys. Plasma* **11** 207

[11] Ding B J, Kuang G L, Shan J F *et al* 2004 *Plasma Phys. Control. Fusion* **46** 1467

[12] Kuang G L, Shan J F, Xu W H *et al* 1999 *Fusion Technol.* **36** 212

[13] Ikeda Y, Imai T, Ushigusa K *et al* 1989 *Nucl. Fusion* **29** 1815

[14] Goniche M, Grosman A, Aniel T *et al* 2004 *Plasma Phys. Control. Fusion* **46** 899

[15] Pericoli R V, Ekedahl A, Erents S K *et al* 2004 *Plasma Phys. Control. Fusion* **46** 349

[16] Mailloux J, Ekedahl, Granucci G *et al* 2004 *ITER relevant coupling of lower hybrid waves in JET Proc. 20th Int. Conf. (Vilamoura, 2004)* IAEA-CN-116/EX/P4-28

[17] Pericoli R V Apicella M L, Barbato E *et al* 2004 *LHCD and coupling experiments with an ITER-like PAM launcher on the FTU tokamak in Fusion Energy 2004 (Proc. 20th Int. Conf. Vilamoura, 2004)* (Vienna: IAEA) CD-ROM file EX/5-5 and http://www-naweb.iaea.org/napc/physics/fec/fec2004/datasets/index.html

[18] Wang M, Liu Y X, Liu F K *et al* 2003 *Nucl. Fusion Plasma Phys.* **23** 55 (in Chinese)

[19] Lilla P in Proc. 2nd Top. Conf. Radiofrequency Plasma Heating (Lubbock, TX, 1974), University of Texas, Austin (1974) paper C3

[20] Xie J K and HT-7 GROUP 1997 *HT-7 superconducting tokamak and its operation in Fusion Energy* 1996 (Proc. 16th Int. Conf. Montreal, 1996) Vol. 1, IAEA, Vienna (1997) 685

[21] Brambilla M 1976 *Nucl. Fusion* **16** 47

[22] Litaudon X Berger-by G, Bibet P *et al* 1992 *Nucl. Fusion* **32** 1883

[23] Ding B J, Kuang G L, Liu Y X *et al* 2002 *Acta Phys. Sin.* **51** 2556 (in Chinese)

[24] Litaudon X and Moreau D 1990 *Nucl. Fusion* **30** 471

[25] Stevens J, Mono M, Horton R and Wilson J R 1981 *Nucl. Fusion* **21** 1259

[26] Fuchs V, Goniche M, Demers Y, Jacquet P and Mailloux J 1996 *Phys. Plasma* **3** 4023

[27] Rantamäki K M, Pättikangas T J H, Karttunen S J *et al* 2000 *Nucl. Fusion* **40** 1477

[28] Goniche M, Guilhem D, Bibet P *et al* 1998 *Nucl. Fusion* **38** 919

[29] Mailloux J, Demers Y, Fucvhs V *et al* 1997 *J. Nucl. Mater.* **241-243** 745

[30] Leuterer F, Söldner F X, Mccormick K *et al* 1991 *Nucl. Fusion* **31** 2315

[31] Karney C F and Fisch N 1985 *Phys. Fluids* **28** 116

[32] Stix T H 1962 *The theory of Plasma Waves* (New York: McGraw-Hill)

[33] SHI B R 1999 *Magnetic Confinement Fusion Principles and Practice* (Atomic Energy Press, Beijing) (in Chinese)
[34] Shi Y J, Chen Z Y, Wan B N *et al* 2004 *Rev. Sci. Instrum.* **75** 4930
[35] EQUIPE TFR 1978 *Nucl Fusion* **18** 647
[36] Tresset G, Litaudon X, Moreau D *et al* 2002 *Nucl. Fusion* **42** 520
[37] Challis C D, Litaudon X, Tresset G *et al* 2002 *Plasma Phys. Control. Fusion* **44** 1031
[38] Joffrin E, Challis C D, Conway G D *et al* 2003 *Nucl. Fusion* **43** 1167
[39] Maget P, Esposito B, Joffrin E *et al* 2003 *Plasma Phys. Control. Fusion* **45** 1385
[40] Garbet X, Bourdelle C, Hoang G T *et al* 2001 *Phys. Plasmas* **8** 2793
[41] Garbet X, Sarazin Y, Ghendrih P *et al* 2002 *Phys. Plasmas* **9** 3893
[42] Budny R, Andre R, Challis C D *et al* 2003 *30th EPS Conf. on Controlled Fusion and Plasma Physics* (St Petersburg, Russia)
[43] Rogister A L 2000 *Phys. Plasmas* **7** 5070
[44] Naito O, Cui Z, Ide S *et al* 2002 *Phys. Rev. Lett.* **89** 065001-1
[45] Joffrin E, Gorini G, Challis C D *et al* 2002 *Plasma Phys. Control. Fusion* **44** 1739
[46] Terry P W 2000 *Rev. Mod. Phys.* **72** 109
[47] LeBlanc B, Batha S, Bell R *et al* 1995 *Phys. Plasmas* **2** 741
[48] Fujita T, Fukuda T, Sakamoto Y *et al* 2004 *Plasma Phys Contr Fusion* **46** A35
[49] Wei W, Ding B J and Kuang G L 2005 *Plasma Sci. Tech.* **7** 2723
[50] Waltz R E 1994 *Phys. Plasmas* **1** 2229
[51] Waltz R E, Kerbel G D, Milovich J and Hammett G W 1995 *Phys. Plasmas* **2** 2408
[52] Biglari H, Diamond P H and Terry P W 1990 *Phys. Fluids* B **2** 1
[53] Itoh K and Itoh S 1996 *Plasma Phys. Control. Fusion* **38** 1